Chapter 5
Gravitational-Wave Astronomy by Precision Laser Interferometry

Norikatsu Mio

Abstract Gravitational waves are the waves of gravitational interaction, which were predicted by Einstein's theory of general relativity. One hundred years after the theoretical prediction, in February 2016, the US LIGO (laser Interferometer Gravitational Wave Observatory) project reported that LIGO had detected a gravitational wave occurring at the coalescence of a black hole binary. Furthermore, the Nobel Prize in Physics in 2017 was awarded to three American physicists who made an outstanding contribution to the LIGO project. Since then, six gravitational wave events have been observed during two observation periods. Moreover, astronomy combined with the observation of electromagnetic waves in a wide wavelength range from radio waves to gamma rays is beginning. In this chapter we will outline the fundamental nature of gravitational waves, their detection method, and this new astronomy.

5.1 Introduction

Gravitational waves (GWs) are the waves of gravitational interaction, which were predicted by Einstein's theory of general relativity (GR)[1] more than 100 years ago. According to GR, a GW appears as strain propagating as a transverse wave with the speed of light. When the theory was proposed, the effect of GWs was considered to be too small to be detected. However, pioneers had started to experimentally investigate the possibility of GW detection in the 1960s. The most famous attempt to detect GWs was by Weber using a cylindrical aluminum body; this detector is known as a Weber bar. He observed the vibration of an elastic mode of the detector. When a GW is incident to the detector, this mode is excited. If the frequency of the GW is close to its resonance, the excitation will be enhanced. In 1969, Weber reported that he could detect GWs; he found coinciding events that were detected by two independent detectors operated at distant locations, one in Maryland and the other in Argonne

[1] The basics on GR are described in the well-known textbook "Gravitation" [1].

N. Mio (✉)
Institute for Photon Science and Technology, University of Tokyo, Bunkyo-ku, Tokyo, Japan
e-mail: mio@ipst.s.u-tokyo.ac.jp

K. Yamanouchi et al. (eds.), *Progress in Photon Science*, Springer Series in Chemical Physics 119, https://doi.org/10.1007/978-3-030-05974-3_5

[2]. After his report, several experiments to confirm his result were performed but no plausible events were detected. In addition, theoretically unreasonable points were found. Thus, Weber's events are not considered to have been GWs. We had to wait a further 50 years before their actual detection. In 2016, the LIGO project announced that they had detected a GW emitted upon the coalescence of a black hole (BH) binary [3].

Since the first detection, six events have been observed: five from BH binaries and one from a neutron star (NS) binary [3–8]. The information obtained from GWs is different from that obtained from observations using an electromagnetic wave (EMW). We are now strongly convinced that GW astronomy is a powerful tool for understanding our Universe.

5.2 Sources of GWs

What can we discover by observing GWs? To discuss this issue, we need to know the mechanism of GW generation. Although a strict discussion requires GR, here we will proceed with a discussion by analogy with EMWs.

EMWs are generated when an electric charge distribution varies with time. For example, charged particles emit an EMW when accelerated, which is derived from the radiation process called electric dipole radiation. An electric dipole moment is defined by

$$\mathbf{p}(t) = \int \mathbf{r}\rho_{\mathrm{e}}(\mathbf{r}, t)\mathrm{d}^3\mathbf{r}, \tag{5.1}$$

where $\rho_{\mathrm{e}}(\mathbf{r}, t)$ is the electric charge distribution. The electric power radiated from a dipole moment is calculated as

$$W = \frac{\mu_0}{6\pi c}\overline{\left|\frac{\mathrm{d}^2\mathbf{p}}{\mathrm{d}t^2}\right|^2}, \tag{5.2}$$

where μ_0 is the vacuum permeability, c is the light velocity [9], and the overline represents the time average.

According to GR, a GW is due to the time variation of the mass distribution $\rho_{\mathrm{m}}(\mathbf{r}, t)$. Since the mass distribution is always positive, the dipole moment always vanishes when we take a centroid coordinate system. Therefore, a GW is generated by the time-dependent mass-quadrupole moment defined by

$$Q_{ij}(t) = \int (x_i x_j - \frac{1}{3}\delta_{ij}r^2)\rho_{\mathrm{m}}(\mathbf{r}, t)\mathrm{d}^3\mathbf{r}, \tag{5.3}$$

where $i, j = 1, 2, 3$ and $x_1 = x, x_2 = y, x_3 = z, r = |\mathbf{r}| = \sqrt{x^2 + y^2 + z^2}$.

The radiation power of a GW can be calculated using the following quadrupole formula:

$$W_{\mathrm{GW}} = \frac{G}{5c^5} \sum_{i,j=1}^{3} \overline{\frac{\mathrm{d}^3 Q_{ij}}{\mathrm{d}t^3} \frac{\mathrm{d}^3 Q_{ij}}{\mathrm{d}t^3}}. \tag{5.4}$$

For example, for the system where two point masses of mass m are performing circular motion with radius a and angular velocity ω around their center of mass, the energy released per unit time is given by

$$W_{\mathrm{GW}} = \frac{128G}{5c^5} m^2 a^4 \omega^6. \tag{5.5}$$

Since gravitational interaction is weak compared with electromagnetic interaction, the energy emitted from artificial objects on the Earth never reaches the detectable level. The energy released from typical objects on the Earth ($a = 1\,\mathrm{m}$, $m = 100\,\mathrm{kg}$, $\omega/2\pi = 100\,\mathrm{Hz}$) is

$$W_{\mathrm{GW}} = 4.3 \times 10^{-31}\,\mathrm{W}. \tag{5.6}$$

The energy emitted during one rotation is calculated as

$$\Delta E = 4.3 \times 10^{-33}\,\mathrm{J} = 0.03\hbar(2\omega). \tag{5.7}$$

Here, $\hbar$ is the Planck constant divided by 2π, and if the gravitational field is quantized, $\hbar(2\omega)$ represents the energy of one quantum.[2] This result shows that it is impossible to effectively generate GWs on the Earth.

Thus, we expect detectable GWs from astronomical objects; the larger the scale concerned, the more dominant the gravitational interaction. As a model calculation of the GW energy from an astronomical phenomenon, we consider a binary system.

Two stars are bound by gravity and move around their center of mass. For simplicity, we consider the case where stars of equal mass are moving circularly. Since the rotation speed is determined by the balance between the centrifugal force and gravitational force, the relation

$$ma\omega^2 = G\frac{m^2}{(2a)^2} \tag{5.8}$$

must be satisfied. Using this formula, we obtain the radiated GW energy as

$$W_{\mathrm{binary}} = \frac{2G^4 m^5}{5c^5} \frac{1}{a^5}. \tag{5.9}$$

This equation shows that the smaller the radius of the orbit the greater the energy released.

[2] The angular frequency of the generated GW is 2ω.

Since the radius is limited by the size of the star, systems that emit a lot of GWs are binaries composed of compact stars such as an NS and a BH.

NSs are thought to be formed by a supernova explosion that produces a core that is made of highly compressed materials mainly composed of neutrons. A typical mass of an NS is considered to be $1.4M_\odot$ and a typical radius is 10 km ($M_\odot$ is the solar mass, 2.0×10^{30} kg). Then, assuming $m = 1.4M_\odot$ and $a = 1000$ km, we obtain $W_{\text{binary}} = 5.6 \times 10^{38}$ W. Since the radiant energy of the Sun is 3.9×10^{26} W, it can be understood that an extremely large amount of energy is released. If this source is at the center of our galaxy (the distance from the earth is about 10 kpc[3]), the energy density on the earth is $4.7 \times 10^{-4}\,\text{W/m}^2$. Sirius, known as a bright star, emits 20 times more energy than the Sun. Since its distance is 2.6 pc, only a photon energy of $9.8 \times 10^{-8}\,\text{W/m}^2$ reaches the Earth.

Despite the very weak gravitational interactions, such a large energy is released because a GW is generated by the movement of the mass of a whole star. Indeed, in the above example, objects of the mass with the Sun move at a speed of 2 % of the light speed.

A GW carries information reflecting the state of motion of such a system. Since the waveform of a GW from a binary system can be predicted, the detection efficiency can be increased by data processing. By analysis of the waveform, it is possible to determine the mass of the original stars, the angular momentum of motion, the state of the star, and so forth, as astronomical information that cannot be obtained from EMWs.

In this system, energy is lost by the emission of GWs, and the state of the orbit changes. Since the total energy of the system is given by

$$E = 2 \times \frac{1}{2} m a^2 \omega^2 - G\frac{m^2}{2a} = -G\frac{m^2}{4a}, \tag{5.10}$$

and the rate of the change in energy is given by (5.9), we obtain

$$\frac{\mathrm{d}E}{\mathrm{d}t} = G\frac{m^2}{4a^2}\frac{\mathrm{d}a}{\mathrm{d}t} = -\frac{2G^4m^5}{5c^5}\frac{1}{a^5}. \tag{5.11}$$

Solving the above equation, we obtain the equation for the change in a as

$$\frac{\mathrm{d}a}{\mathrm{d}t} = -\frac{\Lambda}{4a^3} \tag{5.12}$$

$$\Lambda = \frac{32G^3m^3}{5c^5}. \tag{5.13}$$

Assuming that when $t = t_0$, $a = 0$, we obtain

$$a(t) = [\Lambda(t_0 - t)]^{1/4} \tag{5.14}$$

[3] 1 pc is a distance commonly used in astronomy. 1 pc $= 3.08 \times 10^{16}$ m $= 3.26$ light years.

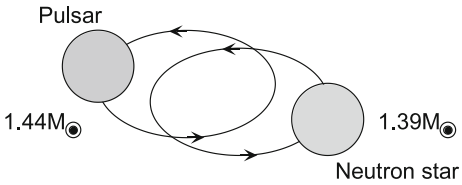

Fig. 5.1 Schematic view of the binary pulsar PSR1913+16

and

$$\omega(t) = \frac{\sqrt{Gm}}{2}[\Lambda(t_0 - t)]^{-3/8}. \tag{5.15}$$

These equations show that a is decreasing as a function of t, while the angular velocity of the rotation is increasing.

The existence of GWs was confirmed by observing such a celestial body. Figure 5.1 is a schematic representation of the NS binary system containing a pulsar called PSR1913+16.

A pulsar is a high-speed rotating NS that generates periodic pulses. However, a large fluctuation was observed in the signal cycle of this pulsar, and it turned out that it is a binary system. Then, by observing the state of the pulse signal, the state of the orbit of the binary system was determined very precisely. The orbital period is about 8 h and the radius of the orbit is approximately the diameter of the Sun (about 10^9 m). Furthermore, it was found that the orbital period of this NS binary is gradually decreasing at a rate of

$$\frac{\mathrm{d}P_{\mathrm{obs}}}{\mathrm{d}t} = (-2.425 \pm 0.002) \times 10^{-12}\,\mathrm{s/s}. \tag{5.16}$$

When calculating the emission energy of the GW using the parameters obtained from the observation, the observed reduction in the orbital period is in good agreement with the theoretical prediction by GR of

$$\frac{\mathrm{d}P_{\mathrm{GR}}}{\mathrm{d}t} = (-2.41958 \pm 0.005) \times 10^{-12}\,\mathrm{s/s}. \tag{5.17}$$

These values coincide with an accuracy of about 0.2% [10]. The Nobel Prize in Physics in 1993 was given to the discoverers of this NS binary.

A variety of relativistic theories of gravity have been proposed since GR was formulated. The observation of GWs is considered to be important for verifying the dynamical properties of theories of gravity [11].

The binary system is continuing to emit GWs. As a result, the two stars will finally merge and will coalesce in about 3×10^8 years.

Just before the coalescence, the orbital cycle will reach millisecond order and a large GW will be generated. All the events that have already been observed are due to this coalescence of the binary system.

5.3 Detection of GWs

How can we actually detect GWs? Since the equivalence principle holds, the effects of gravity on objects that are freely falling vanishes. For a person riding in an elevator freely falling, gravity disappears. However, an elevator has a finite size. If the gravity field is not uniform, the magnitude of the gravity force will be different at the ceiling and the floor. Therefore, we will feel as if we are stretched when we ride on a freely falling elevator. This effect is the same as the force that causes tides and is called the tidal force.

In Newtonian mechanics, two objects at positions $\mathbf{r}$ and $\mathbf{r} + \Delta\mathbf{r}$, they satisfy the following equations of motion:

$$\frac{\mathrm{d}^2\mathbf{r}}{\mathrm{d}t^2} = -\nabla\phi_{\mathrm{g}}(\mathbf{r}), \qquad \frac{\mathrm{d}^2(\mathbf{r}+\Delta\mathbf{r})}{\mathrm{d}t^2} = -\nabla\phi_{\mathrm{g}}(\mathbf{r}+\Delta\mathbf{r}), \tag{5.18}$$

where ϕ_{g} is the Newtonian gravitational potential. Thus, the relative acceleration is given by

$$\Delta\mathbf{a} = \frac{\mathrm{d}^2\Delta\mathbf{r}}{\mathrm{d}t^2} = -[\nabla\phi_{\mathrm{g}}(\mathbf{r}+\Delta\mathbf{r}) - \nabla\phi_{\mathrm{g}}(\mathbf{r})]. \tag{5.19}$$

The right term expresses the tidal force and can be expressed as

$$\Delta a_i = -\sum_{j=1}^{3} \frac{\partial^2\phi_{\mathrm{g}}}{\partial x_i \partial x_j}\Delta x_j \tag{5.20}$$

with the first-order approximation of $\Delta\mathbf{r}$.

If this tidal force is detected, the effect of gravity can be reliably detected. Since the influence of GWs is also known to be tidal, to detect GWs, it is necessary to measure the relative change between the two points.

Figure 5.2 shows the effect of a GW as field lines of the tidal force; these lines of force represent the relative force acting between two points. As mentioned above, a GW is a transverse wave and has two polarization components similarly to EMWs. The polarizations in the two figures have independent components, called the + mode and × mode, which correspond to linear polarizations of EMWs. The polarization of GWs can be expressed as the superposition of + and × modes, similarly to the way that any polarization state of EMWs can be expressed as the superposition of x and y polarizations.

Now considering a GW in the + mode traveling along the z axis with amplitude h, the relative acceleration of two points separated by $(\Delta x, \Delta y)$ in the x–y plane is given by

$$\Delta a_x = \frac{1}{2}\frac{\partial^2 h}{\partial t^2}\Delta x, \qquad \Delta a_y = -\frac{1}{2}\frac{\partial^2 h}{\partial t^2}\Delta y. \tag{5.21}$$

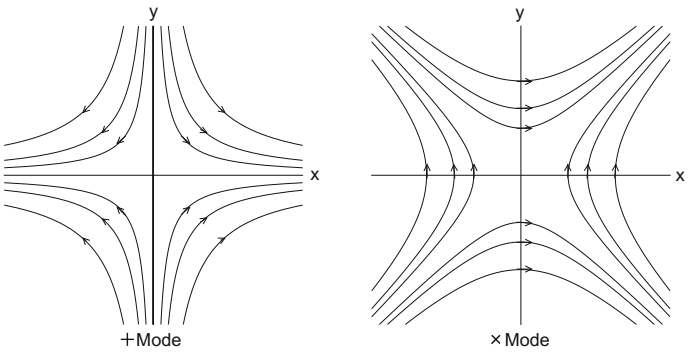

Fig. 5.2 Force lines of GW

For example, if two points separated by L in the x direction on the plane $z = 0$ change their distance by ΔL, $\Delta x = L + \Delta L(t)$ and

$$\Delta a_x = \frac{\mathrm{d}^2 \Delta L}{\mathrm{d}t^2} = \frac{1}{2}\frac{\mathrm{d}^2 h}{\mathrm{d}t^2}(L + \Delta L) \approx \frac{1}{2}\frac{\mathrm{d}^2 h}{\mathrm{d}t^2} L. \tag{5.22}$$

Integrating the above equation with respect to t, we obtain

$$\Delta L = \frac{1}{2} h L. \tag{5.23}$$

Also, in the y direction, the phases of expansion and contraction are inverted. By utilizing this property, we construct a GW detector.

According to a theoretical prediction, the expected value of h is on the order of 10^{-21} or less [12]. If we take L as the distance between the sun and the earth (1.5×10^{11} m), $\Delta L = 7.5 \times 10^{-11}$ m; this is almost the same as the Bohr radius. In other words, it is necessary to detect a relative change that is equivalent to the ratio of the size of a hydrogen atom to the distance between the sun and the earth.

To detect such a weak effect, various detection methods have been developed. Ultimately, laser interferometric detectors successfully detected GWs.

5.4 Laser Interferometric Detectors

As discussed in the previous section, a GW slightly changes the properties of space-time. To detect this effect, we accurately measure the distance between two distant points. For this purpose, a laser interferometer is a powerful tool.

A schematic view of an interferometer is shown in Fig. 5.3. We set two orthogonal optical paths as the x and y axes, When a GW is incident from the direction

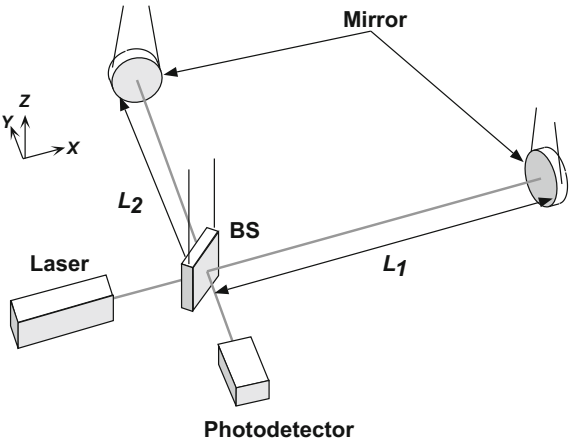

Fig. 5.3 Interferometric GW detector based on Michelson interferometer

perpendicular to the x–y lane (z axis), the x and y directions expand and contract in the x–y plane in opposite directions. A GW oscillates at a certain frequency, which can be observed as a change in the interference fringe of a Michelson interferometer.[4] Mirrors and a beam splitter, which define the optical path length, are suspended similarly to a pendulum. In such a setup, they behave as free masses. By doing so, the interferometer correctly responds to the GW. In addition, it is possible to reduce the influence of external disturbances.

The phase change of the interferometer $\Delta\phi$ is given in terms of the optical path difference $\Delta L_x - \Delta L_y$ as

$$\Delta\phi = \frac{4\pi}{\lambda}(\Delta L_x - \Delta L_y) = \frac{4\pi}{\lambda} hL \tag{5.24}$$

where (5.23) is used to calculate the optical path change as

$$\Delta L_x = -\Delta L_y = hL/2. \tag{5.25}$$

These equations show that the sensitivity increases as the value of L increases. However, if the time for light to travel back and forth through the optical path ($\tau = 2L/c$) becomes longer than a half period of the GW, the phase change due to its effect is integrated and reduced. When τ is on the same order as the period of the GW, the phase change in the Michelson interferometer should be calculated more rigorously using

$$\Delta\phi = \frac{4\pi c}{\lambda\omega} \sin(\omega\tau/2) \exp(-i\omega\tau/2) h_0 \exp(i\omega t). \tag{5.26}$$

[4]Here, we assumed that the GW is polarized in the + mode. In this configuration, the detector has no sensitivity to GWs in the × mode.

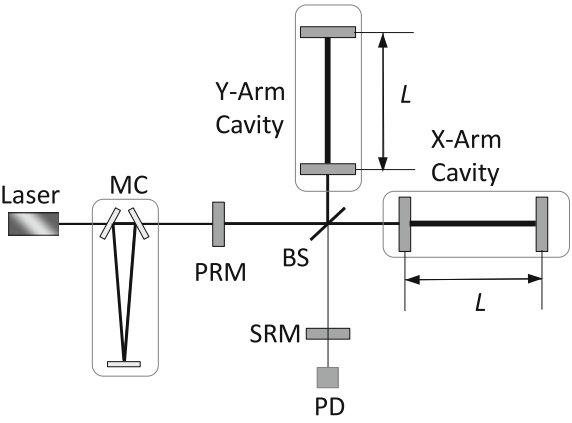

Fig. 5.4 Interferometric GW detector based on Michelson interferometer

Here, we assume that the GW is monochromatic and can be expressed by

$$h(t) = h_0 \exp(i\omega t), \tag{5.27}$$

where ω is the angular frequency of the GW. If $\omega\tau \ll 1$, (5.26) becomes (5.24). Also, from (5.26), $|\Delta\phi|$ becomes maximum if $\omega\tau = \pi$; this gives the optimal condition for the arm length of the interferometer. When we assume that the frequency of the GW is 1 kHz, the optimum value for L is 75 km. In an actual detector, as shown in Fig. 5.4, by incorporating Fabry-Perot optical cavities in both arms of a Michelson interferometer, the sensitivity can be enhanced even for short L of km order. In addition, it is necessary for the laser used as the light source to realize high power and high stability. There is an optical resonator called a mode cleaner (MC) between the interferometer and the laser that shapes the spatial mode of the emitted light and is also used as a reference for frequency stabilization [13]. A power-recycling mirror (PRM) between the MC and the interferometer returns the light to the interferometer again, increasing the effective optical power. It is possible to suppress the influence of shot noise by this technique (called power recycling). There is another recycling mirror at the output port of the beam splitter (BS) called the signal-recycling mirror (SRM), which controls the frequency dependence of the detector sensitivity to GWs. Since very small signals must be measured, to avoid disturbance, the interferometer is housed in a vacuum chamber. The reference mirrors are strictly vibration-isolated. Furthermore, the interferometer requires various control systems so that it can operate stably.

5.5 Noise of the Interferometric Detector

In this section, the noise sources that limit the sensitivity of the interferometer are discussed. In the interferometer, the displacement of the mirror is measured by the interference of light. There are various problems in reading small displacements; any noise source may mask the signal. The main noise sources are shot noise, thermal noise, and seismic noise (Fig. 5.5).

The shot noise determines the smallest detectable change in interference fringes. The shot noise originates from the quantum nature of light, which is a collection of photons; thus, this noise is one of the most fundamental noises. The intensity of light, which is calculated from the number of incident photons N during a unit time, does not become constant because N fluctuates in accordance with quantum effects. The fluctuation of N is given by the square root of N (Poisson process), namely $\delta N = \sqrt{N}$. Since the magnitude of a signal is proportional to N, the signal-to-noise ratio is determined by $N/\sqrt{N} = \sqrt{N}$. Since N is proportional to the power of the light source, a laser with a large power is necessary for the light source to read small changes.

According to detailed calculations, the shot-noise-limited sensitivity of the interferometer to a GW of frequency f is

$$h_{\text{shot}} = 10^{-21} \left(\frac{f}{1\,\text{kHz}} \right) \sqrt{\left(\frac{\lambda}{1\,\mu\text{m}} \right) \left(\frac{1\,\text{kW}}{P} \right) \left(\frac{\Delta f}{1\,\text{kHz}} \right)}, \tag{5.28}$$

where Δf is the bandwidth of the measurement. Here, we assume that a laser with power P at wavelength λ is used with the optimized optical path length.

Ground vibration has a large influence at low frequencies. The ground is continuously shaking even when there is no earthquake. A device (referred to as a vibration

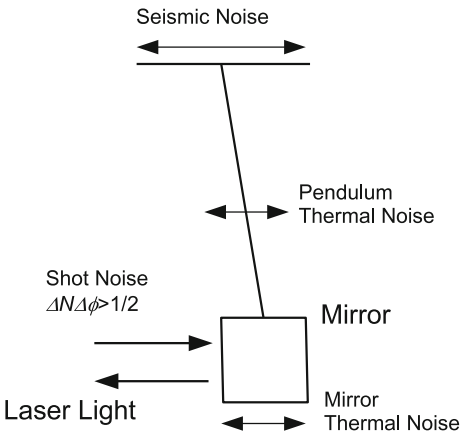

Fig. 5.5 Noise sources of the detector

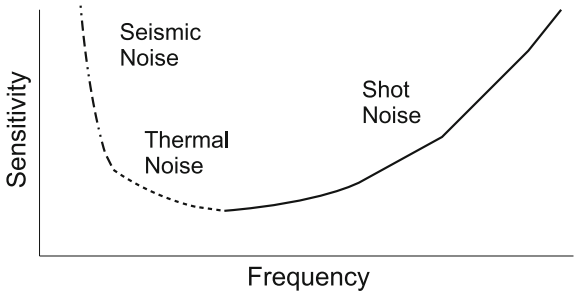

Fig. 5.6 Sensitivity of the detector shown as a function of frequency

isolation system) for blocking this noise can attenuate the magnitude of vibration in the measurement frequency band by a factor of about 10^8.

If the external disturbance is sufficiently removed, the thermal vibrations of the reflection surface of the mirror and the hanging pendulum become the dominant noise sources. These are due to thermal statistical mechanical fluctuation and are also considered also as a principal source of noise.

To reduce this noise, the most direct method is to lower the temperature. In addition, it is necessary to select materials with low mechanical loss. For this reason, high-purity synthetic silica is currently used. For the low-temperature environment, sapphire or other monocrystalline substrates must be used. The properties of single-crystal sapphire have been studied for use in the KAGRA interferometer being constructed.

The dominant noise changes with the frequency. At low frequencies (10 Hz or less), ground vibration is the largest noise. At intermediate frequencies (10–100 Hz order), thermal noise is high. At higher frequencies, shot noise becomes the main noise source. Figure 5.6 represents a schematic sensitivity curve limited by the noise source of the interferometer as a function of frequency.

5.6 Major Projects

An interferometer that can actually detect GWs is extremely large; such an interferometer is qualitatively different from ordinary optical devices used in laboratories. The construction of such an interferometer is a major project requiring a large amount of human resources, a huge budget and a very long time.

The LIGO project has two 4-km interferometers that have been constructed on the east coast (Livingstone, Louisiana) and west coast (Hanford, Washington) of the US. The budget was approved in 1990 and the construction began in 1992. In the autumn of 2000, the first interference fringe was observed. After that, the system, called initial LIGO, achieved its designed sensitivity in 2005. Advanced LIGO started in 2008, in which new vibration isolation systems, new mirrors, new lasers, and so forth

Table 5.1 Web sites of GW projects

LIGO	http://www.ligo.caltech.edu/
LSC	https://www.ligo.org/
VIRGO	http://www.virgo-gw.eu/
KAGRA	http://gwcenter.icrr.u-tokyo.ac.jp/en/

were developed and installed to the detectors. These efforts resulted in the successful detection of GWs [14].

In Europe, France and Italy are collaborating to build a detector named VIRGO, located near Pisa in Italy, with an interferometer of length 3 km. To detect low-frequency GWs, a special vibration isolation device was being introduced.

LIGO and VIRGO are now working together as LIGO-VIRGO collaboration. The first detection of a GW was simultaneously announced in the US and Europe.

In Japan, a 3-km interferometer named KAGRA is being constructed inside Kamioka mine. Many research institutes are participating.

The web URLs of these projects are shown in Table 5.1. For details, see these web pages.

5.7 KAGRA

Here, the Japanese project KAGRA is discussed [15]. This project was started in 2010 with the aim of constructing a 3-km-long interferometer at the underground site of Kamioka mine in Gifu prefecture, shown in Fig. 5.7.

To suppress thermal noise, a cryogenic technology to cool the arm mirrors has been introduced. Owing to their suitability for use in a cryogenic environment, large sapphire crystals are used as substrates for the arm mirrors. The target sensitivity is sufficient to detect GWs from the coalescence of an NS binary. When the KAGRA detector is operated, it will provide valuable information to the worldwide network of GW detectors because the distant location of KAGRA from the other detectors is advantageous in determining direction of the GW sources.

The construction of the tunnel of KAGRA was finished in 2014 and the huge vacuum system was installed. The first trial to obtain an interference signal was carried out in 2016, which was successful [16]. After that, the cryogenic system was installed. In 2018, an end test mass made of a single-crystal sapphire was installed in the KAGRA system. The first trial operation of the cryogenic interferometer without arm cavities has started in May 2018.

KAGRA requires many advanced technologies concerning optics, mechanics, cryogenics, control systems, and so forth. Our group is working on the development of the light source for KAGRA. In the following section, we describe the light source.

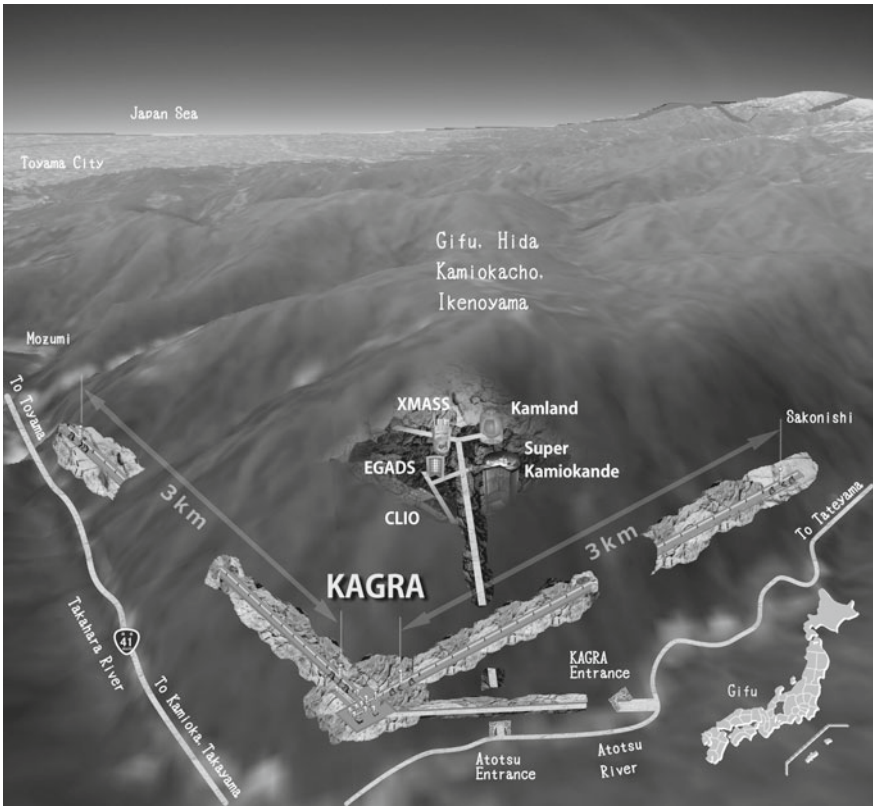

Fig. 5.7 Overview of KAGRA (offered by Shinji Miyoki at ICRR, the University of Tokyo)

5.8 Light Source for KAGRA

To realize the target sensitivity of KAGRA, the noise level must be controlled to the target value. For shot noise, the laser power limits the noise level and must be larger than 180 W with single-frequency and single-mode CW oscillation assuming a laser wave length of 1064 nm. There are two ways of realizing such laser oscillation: one is to use a master oscillator and power amplifier (MOPA) and the other is by injection locking. We have developed a laser system based on injection locking and achieved a 100 W single-frequency output [17, 18]. However, the injection-locking system requires a servo control system to maintain the injection-locked state and needs fine tuning in alignment. Since the complexity of the allover detector system should be minimized, we adopted a MOPA system for KAGRA. A schematic view of the KAGRA laser system is shown in Fig. 5.8; the system consists of a seed laser (NPRO), two fiber-laser amplifiers, and a three-stage solid-state laser amplifier.

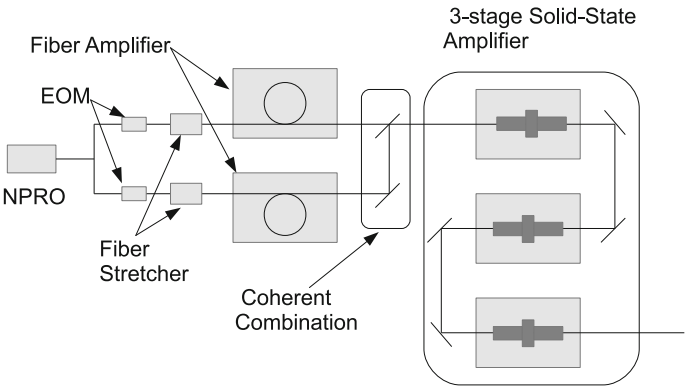

Fig. 5.8 Laser system for KAGRA

The seed laser emits a small power (about 400 mW) with very high frequency stability at 1064 nm. The output of the seed laser is divided into two optical paths using an optical-fiber-based system. An EOM and a fiber stretcher are placed on each optical path to control the phase of the laser light. The two outputs of the divided optical paths are introduced into two fiber-laser amplifiers with 40 W output power. These two laser beams are coherently combined to obtain a higher power than that necessary for the solid-state laser to work in the saturated amplification regime. After the coherent combination, the laser light is incident to the three-stage solid-state amplifier, which is composed of LD-pumped Nd:YAG laser modules. As mentioned above, by adopting the MOPA scheme, the operation of the laser becomes easier than that based on injection locking. Also, we can use fiber laser technology, which enables high-quality amplification. However, narrow-band amplification with a fiber laser sometimes becomes unstable because of nonlinear effects, mostly stimulated Brillouin scattering. Thus, single-frequency amplification to the level required for KAGRA is very difficult and we adopted a simple solid-state laser for the last stage of amplification. We have succeeded in high-efficiency coherent combination. As shown in Fig. 5.9, we obtained 78 W output from two 41 W outputs with a good optical mode. The efficiency of the coherent combination was 95 %.

Although we have also performed amplification using the solid-state laser, the output power with the fundamental optical mode was limited to about 150 W, which is not sufficient for use in KAGRA. We are currently considering how to improve the system to obtain the target laser power.

Regarding the frequency noise, we have confirmed that the noise level of the combined and amplified output was almost the same as that of the NPRO as shown in Fig. 5.10.

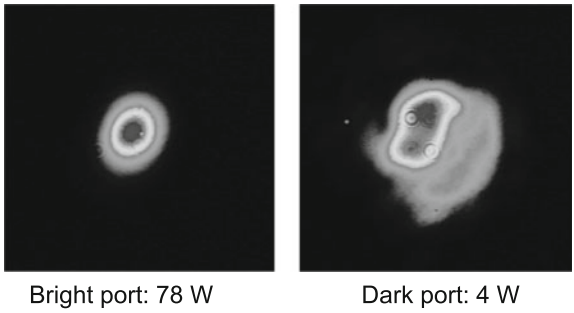

Fig. 5.9 Results of the coherent combination

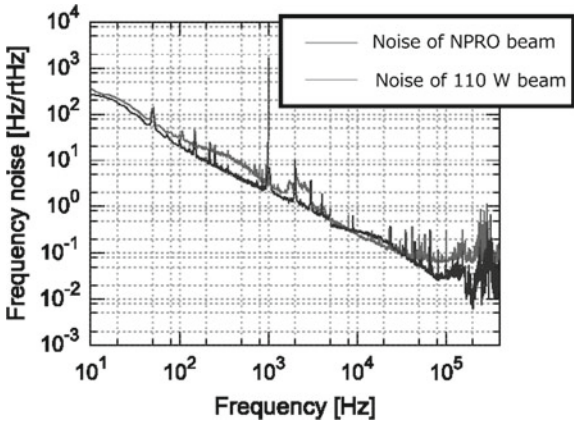

Fig. 5.10 Frequency noise of the laser system

5.9 GW Astronomy

Observation using GWs can clarify the state of motion of a global mass that cannot be determined by other means; this is the most advantageous feature of GW astronomy.

However, the detection of GWs is extremely rare. To obtain a sufficient observation rate (several times a year), we have to observe a wide area of the Universe, and sufficient sensitivity to observe very distant objects is necessary.

Actually, before the first detection of GWs, their most promising source was considered to be the coalescence of NS binaries. Furthermore, from the event rate estimated on basis of the observations of the NS binaries, GWs can be detected several times a year using detectors with a detection distance of about 200 Mpc.

However, the first event for which GWs were observed was BH binary coalescence. BHs of $36\,M_\odot$ and $29\ M_\odot$ located at a distance of 410 Mpc from the Earth merged into a single BH of $62\,M_\odot$. The energy of the emitted GW was about $3\,M_\odot c^2$; a very large amount of energy was carried by the GW. The detected amplitude of the GW at LIGO was about 10^{-21}. This was the first proof that BH binaries really exist. The masses of the BHs observed here were heavy; the masses of stellar-mass BHs observed before the first GW detection were smaller than $20\,M_\odot$.

Since the first detection, six events have been observed in two observation runs of LIGO and VIRGO. Five of the events were the coalescence of BH binaries. In addition, the coalescence of an NS binary has also been observed; this occurred at a distance of 44 Mpc, which was much closer than expected. From these findings, we consider that the prediction of the abundance of GW sources before the actual detector operation was very conservative; the population of possible sources of GWs seems to be much larger than previously estimated. Regarding the mass of the observed BHs, we found that the BH masses are extremely large among the stellar-mass BHs observed so far; the in-depth understanding of the evolution of BHs is expected to rapidly increase as a result of GW observations.

With regard to the observed coalescence of the NS binary, gamma rays were detected at almost the same time, which arrived at the Earth with 1.7 s delay; this indicates that the speed of GWs coincides with that of EMWs within an uncertainty of $(^{-3}_{+0.7}) \times 10^{-15}$ [19]. This is the first time that the speed of GWs has been experimentally determined.

Moreover, since the direction of a celestial source was first determined from the signal of a GW, observations of the source have been carried out with a wide range of EMWs. The Hubble constant H_0 has been estimated as $H_0 = 70.0^{+12.0}_{-7.0}$ km/s/Mpc on the basis of these observations; this is consistent with previously determined values [20].

A new astronomy, called multi-messenger astronomy involving the simultaneous observation of GWs and EMWs has been developed and is providing valuable results.

5.10 Summary

GW astronomy is in its infancy. In the period of over two years since the first observation of GWs, there have been six further observations, and the information obtained could not have been obtained by other means. Their simultaneous observation with EMWs has already been achieved, providing new knowledge on the Universe. Advanced photon science and technology have played an important role in the detection and will continue to contribute to improving detection sensitivity.

References

1. C.W. Misner, K.S. Thorne, J.A. Wheeler, Gravitation (W. H. Freeman, San Francisco, 1973), ISBN: 978-0-7167-0344-0
2. J. Weber, Evidence for discovery of gravitational radiation. Phys. Rev. Lett. **22**, 1320 (1969)
3. B.P. Abbott et al., (LIGO scientific collaboration and virgo collaboration) (11 Feb 2016), Observation of gravitational waves from a binary black hole merger. Phys. Rev. Lett. **116**, 061102 (2016)

4. B.P. Abbott et al., (LIGO scientific collaboration and virgo collaboration) (15 June 2016), GW151226: observation of gravitational waves from a 22-solar-mass binary black hole coalescence. Phys. Rev. Lett. **116**, 241103 (2016)
5. B.P. Abbott et al., (LIGO scientific collaboration and virgo collaboration) (1 June 2017). GW170104: observation of a 50-solar-mass binary black hole coalescence at redshift 0.2. Phys. Rev. Lett. **118**, 221101 (2017)
6. B.P. Abbott et al., (LIGO scientific collaboration and virgo collaboration) (18 Dec 2017). GW170608: observation of a 19-solar-mass binary black hole coalescence. Astrophys. J. Lett. **851**, L35 (2017)
7. B.P. Abbott et al., (LIGO scientific collaboration and virgo collaboration) (6 Oct 2017) GW170814: a three-detector observation of gravitational waves from a binary black hole coalescence. Phys. Rev. Lett. **119**, 141101 (2017)
8. B.P. Abbott et al., (LIGO scientific collaboration and virgo collaboration) (16 Oct 2017). GW170817: observation of gravitational waves from a binary neutron star inspiral. Phys. Rev. Lett. **119**, 161101 (2016)
9. J.D. Jackson, *Classical Electrodynamics*, Third Edition (Wiley, New York, 1999), ISBN: 0-471-30932-X, OCLC 925677836
10. J.M. Weisberg, J.H. Taylor, in *The Relativistic Binary Pulsar B1913+16: Thirty Years of Observations and Analysis*, ed. by F. A. Rasio, I.H. Stairs. Binary radio pulsars, ASP conference series, vol. 328, proceedings of conference held 11–17 Jan 2004, Aspen, Colorado, USA (Astronomical Society of the Pacific, San Francisco, 2005), p. 25
11. C.M. Will, The confrontation between general relativity and experiment. Living Rev. Relativ. (https://link.springer.com/article/10.12942/lrr-2014-4)
12. K.S. Thone, Gravitational radiation, in *Three Hundred Years of Gravitation*, ed. by S. Hawking, W. Israel (Cambridge University Press, Cambridge, New York, 1987), pp. 300–458
13. S. Reid, S. Rowan, J. Hough, Gravitational wave detection by interferometry (ground and space). Living Rev. Relativ. (https://link.springer.com/article/10.12942/lrr-2011-5)
14. J. Aasi et al., Advanced LIGO. Class. Quantum Grav. **32**, 074001 (2015)
15. T. Akutsu et al., Construction of KAGRA: an underground gravitational-wave observatory. Prog. Theor. Exp. Phys. **2018**, 013F01 (2018)
16. T. Akutsu, KAGRA Collaboration, Large-scale cryogenic gravitational-wave telescope in Japan: KAGRA., J. Phys. Conf. Ser. **610**, 012016 (2015)
17. K. Takeno, T. Ozeki, S. Moriwaki, N. Mio, 100 W, single-frequency operation of an injection-locked Nd:YAG laser. Opt. Lett. **30**, 2110 (2005)
18. N. Ohmae, S. Moriwaki, N. Mio, Wideband and high-gain frequency stabilization of a 100-W injection-locked Nd:YAG laser for second-generation gravitational wave detectors. Rev. Sci. Instrum. **81**, 073105 (2010)
19. B.P. Abbott et al., (LIGO scientific collaboration and virgo collaboration), Gravitational waves and gamma-rays from a binary neutron star merger: GW170817 and GRB 170817A. Astrophys. J. Lett. **848**, L13 (2017)
20. The LIGO Scientific Collaboration and The Virgo Collaboration, The 1M2H Collaboration, The Dark Energy Camera GW-EM Collaboration and the DES Collaboration, The DLT40 Collaboration, The Las Cumbres Observatory Collaboration, The VINROUGE Collaboration & The MASTER Collaboration, A gravitational-wave standard siren measurement of the Hubble constant. Nature **551**, 85 (2017). https://doi.org/10.1038/nature24471